

# The Phenoxy Radical–Water Complex—A Matrix Isolation and Computational Study

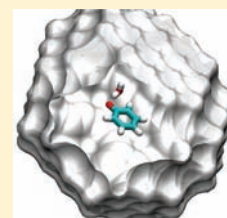
Wolfram Sander,<sup>\*,†</sup> Saonli Roy,<sup>†</sup> Iakov Polyak,<sup>‡</sup> Juan Manuel Ramirez-Anguila,<sup>‡</sup> and Elsa Sanchez-Garcia<sup>\*,‡</sup>

<sup>†</sup>Lehrstuhl für Organische Chemie II, Ruhr-Universität Bochum, D-44801 Bochum, Germany

<sup>‡</sup>Max-Planck-Institut für Kohlenforschung, Kaiser-Wilhelm-Platz 1, D-45470 Mülheim an der Ruhr, Germany

**S** Supporting Information

**ABSTRACT:** The phenoxy radical **1** was generated in high yields by flash vacuum pyrolysis of allyl phenyl ether **2** with subsequent trapping of the products in argon at 3 K. In water-doped argon matrices, an OH...O complex between **1** and water is formed that could be characterized by IR spectroscopy. Several isotopomers of the complex were generated, and the IR spectra compared to results of density functional theory calculations. Other dimers between **1** and water were not found under these conditions. QM/MM calculations in simulated argon matrices reveal that an OH... $\pi$  complex is unstable even at a time scale of picoseconds. This finding has implications on the related interaction between the tyrosyl radical and the water in biological systems.



## ■ INTRODUCTION

Hydrogen bonding is the most important of the “weak” intermolecular interactions and has been studied extensively both experimentally and theoretically.<sup>1,2</sup> The interaction between a hydrogen bond donor X–H (an electron-deficient hydrogen atom) and acceptor Y (an electron-rich area of the molecule) results in a transfer of charge from the acceptor to the donor in the resulting X–H–Y bond. Typical acceptors Y are atoms with lone pairs such as nitrogen or oxygen but also  $\pi$ -systems such as aromatic systems or alkynes. Hydrogen bonds with carbon atoms as acceptors are limited to  $\pi$ -systems or carbanions, with the latter being very powerful acceptors. However, because of their high basicity, hydrogen bonding to carbanions frequently leads to a complete hydrogen transfer, and thus protonation of the carbanion.

Radicals are in principle also capable of accepting hydrogen bonds, although to a lesser extent.<sup>3–11</sup> Previous theoretical studies indicate that indeed radical centers can act as weak hydrogen bond acceptors.<sup>3,7–9,12,13</sup> There is a principal difference between hydrogen bonding to closed shell molecules and to radicals: whereas a “normal” hydrogen bond can be looked upon as an intermediate along the reaction coordinate resulting in proton transfer, hydrogen-bonded radicals are intermediates toward hydrogen atom transfer, although proton transfer can also be an option. There are only few experimental studies of radicals as hydrogen bond acceptors.<sup>3–6,10,11,14–16</sup> For the phenyl radical interacting with water, an OH... $\pi$  complex was found under the conditions of matrix isolation.<sup>5,11</sup> This complex is thermally and photochemically highly labile, and excitation with visible light results in the formation of a  $\pi$ -complex between the hydroxyl radical and the benzene. Thus, a hydrogen atom is transferred from water to the phenyl radical.

The phenoxy radical **1** is a delocalized  $\pi$ -radical and therefore more stable than the phenyl radical (in terms of bond dissociation energies for the hydrogen abstraction from

benzene and phenol, respectively). The water complex of the phenoxy radical is of particular interest because of its relation to the tyrosyl radical, which is one of the most important radicals in biological systems.<sup>17</sup> The tyrosyl radical is formed by oxidation of the redox-active amino acid tyrosin by oxidants such as cytochrome *c* and plays a vital role in key biochemical processes such as the formation of deoxyribonucleotides from ribonucleotides in the ribonucleotide reductase<sup>18</sup> or in the water-oxidizing enzyme of photosynthesis, photosystem II (PSII).<sup>19–21</sup> In the PSII, the tyrosyl radical is bound to a manganese cluster and is interacting with two water molecules. The hydrogen atom transfer from water to tyrosyl is a key step in the oxygen generation process of PSII. Not much attention has been drawn to the interaction between the radical center and the water. A weakly bound complex between water and tyrosyl could play an active role in the hydrogen atom transfer. As a model for this, we use a complex between the related phenoxy radical and the water, which was prepared and spectroscopically characterized under the conditions of matrix isolation.

A number of spectroscopic studies of radical **1** have been published, including IR, resonance Raman, UV–vis, EPR, and ENDOR spectroscopy.<sup>22–28</sup> In a very careful study, Radziszewski et al. assigned the IR spectrum of matrix-isolated **1** and several of its isotopomers.<sup>29</sup> Radical **1** was generated in argon at 7–10 K by UV irradiation of a variety of precursors, such as nitrosobenzene, nitrobenzene, diphenylperoxide, or phenol. The disadvantage of the generation of **1** by photolysis of a matrix-isolated precursor is that radical pairs are formed inside matrix cages that have a high tendency of recombination. In particular, any annealing of the matrix, which is necessary to

Received: February 26, 2012

Published: April 6, 2012

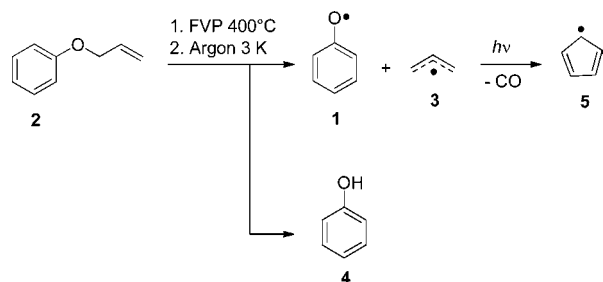
induce diffusion and thus bimolecular reactions of radicals with other trapped molecules, results in recombination.

We therefore generate **1** in the gas phase by flash vacuum pyrolysis (FVP) of a suitable precursor and subsequently trap **1** (and the other products formed during FVP) in a low-temperature matrix. This results in radical species trapped in individual matrix cages, and the loss of radicals due to recombination of radical pairs is much lower. It has been shown previously that the pyrolysis of anisole using a hyperthermal nozzle indeed results in the formation of the phenoxy radical **1**;<sup>29</sup> however, the yield is limited by incomplete conversion at lower temperatures and decarbonylation to produce the cyclopentadienyl radical at higher temperatures. A suitable precursor of **1**, which decomposes at much lower temperatures than anisole, is allyl phenyl ether **2**.<sup>31</sup> The lower pyrolysis temperatures result in less decarbonylation and thus higher yields of **1**.

## RESULTS AND DISCUSSION

**Matrix IR Spectra.** FVP of allyl phenyl ether **2** at 400 °C with subsequent trapping of the products in argon at 3 or 10 K produces the phenoxy radical **1** together with the allyl radical **3** and phenol **4** (Scheme 1). These products were identified by

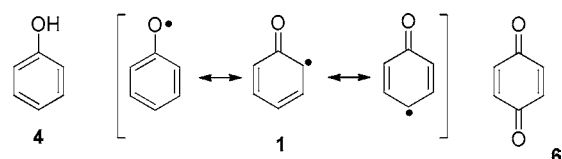
Scheme 1. FVP of Allyl Phenyl Ether **2**



comparing the matrix IR spectrum of the FVP products (Figure S1 in the Supporting Information) with published spectra of **1**,<sup>29</sup> **3**,<sup>32</sup> and **4**.<sup>28,33</sup> FVP at higher temperatures in addition produced the cyclopentadienyl radical **5** and CO. UV photolysis of matrices containing radical **1** also produces **5** and CO, in accordance with the literature.<sup>31</sup> If *d*<sub>5</sub>-**2** with the phenyl ring perdeuterated is used as a precursor, a mixture of *d*<sub>5</sub>-**4** and *d*<sub>6</sub>-**4** is formed, in addition to the expected *d*<sub>5</sub>-**1**.

To enable the formation of complexes of **1** with water, the products of the FVP of **2** were trapped in argon doped with 0.1–1% water. After deposition of the matrix at 3–10 K, the matrix was annealed at temperatures between 25 and 35 K. At these temperatures, small molecules are able to diffuse in solid argon, and the formation of aggregates can be directly followed by IR spectroscopy.<sup>34</sup> The formation of aggregates is a complex process and depends strongly on (i) the concentration of the molecules trapped in argon, (ii) the deposition temperature, and (iii) the annealing temperature. Thus, with 0.1% water in argon, matrices are formed that contain isolated water molecules but also dimers, trimers, and higher oligomers.<sup>35,36</sup> With an increasing concentration of water, the concentration of oligomers increases, as expected. We also found that at the same concentration of water in argon, less oligomers are observed if the matrix is deposited at 3 K instead of 10 K or higher temperatures. Obviously, even at 10 K, water is aggregating during the formation of the matrix, whereas at 3 K, the cooling of the gas mixture deposited from the gas phase on the matrix window is so fast that aggregation is minimized.

Annealing of argon matrices containing both **1** and water results in the formation of a new set of IR absorptions, which is



not observed if the argon is doped with only **1** or with only water. These new absorptions resemble the vibrations of the monomers but are either red- or blue-shifted with respect to the corresponding monomer bands. These shifts in monomer absorptions are characteristic of weakly bound aggregates. An additional mode, which does not exist in either of the monomers, is assigned to an intermolecular vibration of a complex between **1** and water. By variation of the concentration of water in the matrix and carefully studying the changes in the spectra, we conclude that a dimeric complex between **1** and water is formed during the annealing of the matrix. At very low concentrations of water (0.1%) and if the matrix is deposited at very low temperatures (3 K), mostly monomers (water and **1**) are found in the matrix. Higher concentrations of water (1%) or deposition of the matrix at higher temperatures (10 K) results in the formation of larger amounts of the dimer. Annealing of

Table 1. Vibrational Frequencies and Shifts of the Phenoxy Radical–Water Dimer A

argon, 10 K <sup>a</sup> $\nu$ , cm <sup>-1</sup> (rel. I)	shift <sup>b</sup>	calcd gas phase <sup>c</sup> $\nu$ , cm <sup>-1</sup> (I, km/mol)	shift <sup>b</sup>	calcd argon <sup>d</sup> $\nu$ , cm <sup>-1</sup>	shift <sup>b</sup>	assignment
3470.5 (100) <sup>e</sup>	-167.5	3724.0 (540)	-169.2	3608	-192	water OH str. (sym)
1553.3 (33)	+3.5	1628.9 (72)	+1.6	1585	+3	CC str.
1495.1 (28)	+14.6	1540.5 (78)	+30.8	1502	+22	CO str.
1517.0 (18)	+3.8	1591.1 (5)	-1.8	1546	+4	CC str./CH bend
1323.9 (12)	+6.3	1361.6 (7)	+6.3	1346	+12	CC str./CH bend
905.7 (10)	+7.1	957.9 (11)	+6.8	945	+11	CH o.o.p. wag
787.8 (47)	+3.2	821.8 (26)	+7.2	809	+5	CH o.o.p. wag
		827.0 (20)	+12.4			
637.0 (56)	+1.5	660.3 (53)	+6.1	660	+3	CH o.o.p. wag
358.9 (25)		395.6 (200)		387		water rocking

<sup>a</sup>Frequencies (cm<sup>-1</sup>), relative intensities based on the strongest absorption in parentheses. <sup>b</sup>Frequency shift relative to the monomers (cm<sup>-1</sup>). <sup>c</sup>UM052X/6-311++G(2d,2p), intensities in parentheses. <sup>d</sup>QM (UB3LYP-D2/TZVPP)/CHARMM. <sup>e</sup>Only the shift of the symmetrical OH str. vibration was observed. The two other water vibrations are calculated to show much smaller shifts that could not be observed due to overlapping bands.

the matrix at 35 K results in a decrease of the monomers of **1** and water and simultaneously in an increase of the dimer.

The largest shift in the dimer is found for the OH stretching vibration of water, which is red-shifted by  $167\text{ cm}^{-1}$  from  $3638^{64,65}$  to  $3471\text{ cm}^{-1}$  (Table 1 and Figure 1). The new band

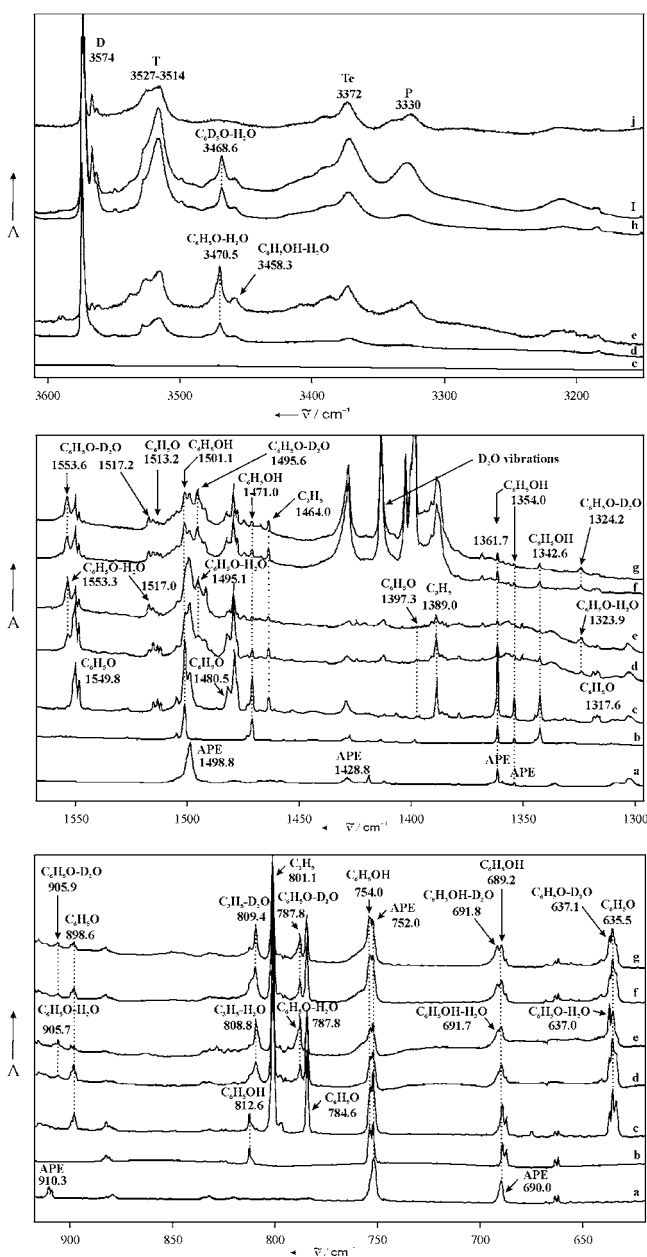


**Figure 1.** IR spectra ( $3600\text{--}600\text{ cm}^{-1}$ ) of argon matrices showing the formation of the dimer between **1** and water. (a) Precursor **2** at 10 K. (b) Phenol at 10 K. (c) FVP products of **2** trapped in argon at 3 K. (d) FVP products of **2** trapped in argon doped with 1% water at 3 K. (e) Same matrix as d after annealing to 35 K for several minutes and cooling down to 3 K. (f) FVP products of **2** trapped in argon doped with 1%  $\text{D}_2\text{O}$  at 3 K. (g) Same matrix as f after annealing to 35 K for several minutes and cooling down to 3 K. (h) FVP products of  $d_5$ -**2** trapped in argon doped with 1% water at 3 K. (i) Same matrix as h after annealing to 35 K for several minutes and cooling down to 3 K. (j) One percent water at 3 K. D, water dimer; T, water trimer; Te, water tetramer; and P, water polymer.

at  $3471\text{ cm}^{-1}$  is clearly different from the absorptions of water oligomers,<sup>35–38</sup> phenol, phenol–water complexes,<sup>33</sup> or the

complex between the allyl radical **3** and the water.<sup>39</sup> If  $\text{D}_2\text{O}$  is used to form the dimer, a new band at  $2551\text{ cm}^{-1}$  is found, red-shifted from the O–D stretching vibration of  $\text{D}_2\text{O}$  by  $108\text{ cm}^{-1}$ . This very large red shift clearly indicates that water acts as hydrogen bond donor in the dimer between **1** and water. The formation of the water complex also results in shifts of several bands of the phenoxyl radical **1** (Table 1). Interestingly, only blue shifts are observed. The largest shift is found for the CO stretching vibration at  $1481\text{ cm}^{-1}$ , which is blue-shifted by  $15\text{ cm}^{-1}$ . This indicates that the oxygen atom is strongly involved in the stabilization of the dimer. The frequency of the CO stretching vibration of **1** is about half way between that of *p*-benzoquinone **6** (argon matrix,  $1672\text{ cm}^{-1}$ )<sup>40</sup> and phenol **4** (argon matrix,  $1257\text{ cm}^{-1}$ ),<sup>33</sup> indicating a partial double bond character of this bond, in accordance with the resonance structures of **1**.

However, in general, the formation of hydrogen bonds with a carbonyl oxygen atom as hydrogen bond acceptor leads to a strong red shift of the CO stretching vibration. The large blue shift observed in the complex of **1** with water is therefore unusual. The blue shifts observed for the other vibrations upon formation of the  $\text{1}\cdots\text{H}_2\text{O}$  complex are smaller. Shifts of  $6.3$  and  $7.1\text{ cm}^{-1}$  are found for the absorptions at  $1324$  and  $906\text{ cm}^{-1}$ , respectively, and for the other bands, the shifts are below  $4\text{ cm}^{-1}$  (Table 1).

Highly characteristic for the dimer between **1** and water is an intermolecular mode at  $359\text{ cm}^{-1}$ , which is neither found in **1** nor in water (Table 1 and Figure 2). Similar vibrations are observed for other water complexes and are described best as rocking vibrations of a water molecule hydrogen-bonded to another acceptor molecule, for example, in the water dimer. By comparison with the water complexes of the other products in the matrix, we could exclude that this vibration is caused by

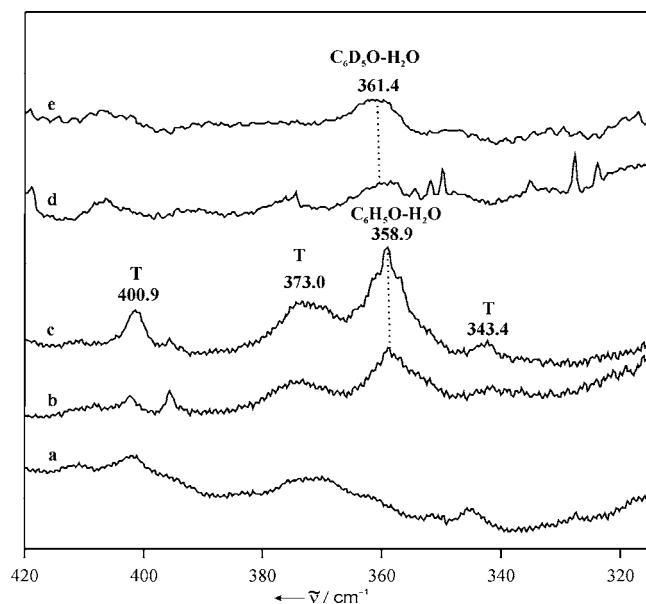


**Figure 2.** IR spectra ( $300\text{--}400\text{ cm}^{-1}$ ) of argon matrices showing the formation of the dimer between **1** and water. (a) One percent water in argon at 3 K. (b) FVP products of **2** trapped in 1% water/argon at 3 K. (c) After annealing to 35 K for several minutes and cooling down to 3 K. (d) FVP products of  $d_5$ -**2** trapped in argon doped with 1% water at 3 K. (e) After annealing to 35 K for several minutes and cooling down to 3 K. Bands marked T are assigned to water trimers.

water oligomers, phenol–water aggregates, or other water complexes.

The observed strong red shift of the symmetrical OH stretching vibration of water and the observation of an intermolecular rocking vibration of water suggest that water acts as hydrogen bond donor in the  $\text{I}\cdots\text{H}_2\text{O}$  dimer. In principle, both the  $\pi$ -system of **1** or the lone pairs at the phenoxy oxygen atom could serve as a hydrogen bond acceptor. If the oxygen atom is involved, we expect a red shift of the CO stretching vibration as found in hydrogen-bonded carbonyl compounds. A  $\pi$ -complex should affect the CO stretch to a much lesser extent. The large blue shift observed indicates that the phenoxy oxygen atom is directly involved in the interaction with the water molecule; however, to find a blue shift instead of a red shift is unexpected.

**DFT Calculations.** Two phenoxy radical–water dimers **A** and **B** (Figure 3) are identified at the DFT level of theory using

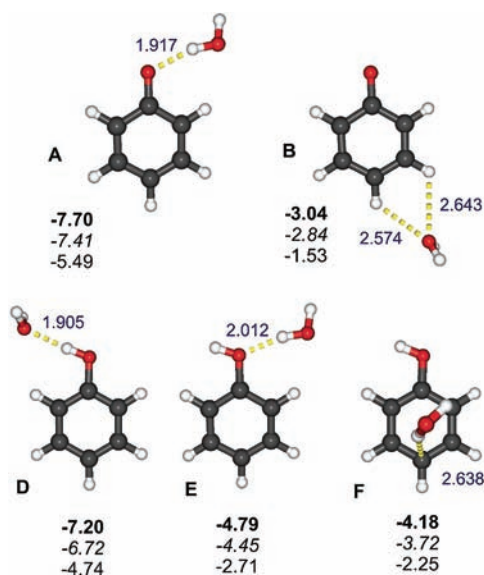


**Figure 3.** Geometries and dissociation energies of the dimers **A** and **B** between the phenoxy radical and the water and the dimers **D**, **E**, and **F** between phenol and water, calculated at the UM05-2X/6-311+G(2d,2p) level of theory. Energies (kcal/mol) are shown without corrections (bold), including BSSE corrections (italics) and including both BSSE and ZPE corrections. Nonbonding distances in blue (Å).

the B3LYP-D2<sup>41–45</sup> and M05-2X<sup>46</sup> density functionals. The most stable dimer **A** [–7.41 kcal/mol, UM05-2X/6-311+G(2d,2p) +BSSE] is stabilized by an  $\text{OH}_{\text{water}}\cdots\text{O}_{\text{radical}}$  hydrogen bond with an  $\text{H}\cdots\text{O}$  distance of 1.917 Å (Figure 3). Dimer **B** is a van der Waals complex with a very weak (–2.84 kcal/mol)  $\text{O}_{\text{water}}\cdots\text{CH}_{\text{radical}}$  interaction (Figure 3 and Table S2 in the Supporting Information). Unlike in the phenol–water system,<sup>33</sup> an  $\text{OH}\cdots\pi$  complex could not be located in the phenoxy radical–water system. Optimization of any structure with a water molecule positioned on top of the  $\pi$  system of **1** rapidly converged to dimer **A**. To clarify this observation, dynamic calculations have been carried out in the gas phase and in a simulated argon matrix (see the following).

Because the abstraction of a hydrogen atom from water by radical **1** is strongly endothermic, this reaction does not occur at low temperatures. We also have no evidence for a photochemical hydrogen abstraction, as was previously found for the phenyl radical.<sup>5,11</sup> However, the reverse reaction

between an OH radical and a phenol is of considerable interest, and we therefore calculated the intrinsic reaction coordinate (IRC) for this hydrogen transfer reaction at the UM052x/6-311+g(2d,2p) level of theory (Figure 4). In the

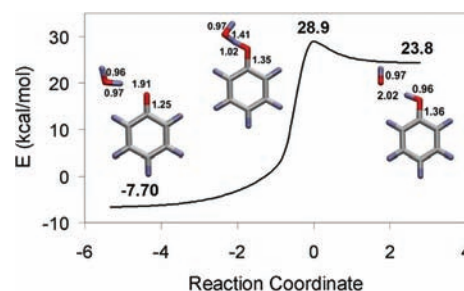


**Figure 4.** Hydrogen abstraction reaction pathway (IRC) in the phenoxy radical–water system calculated at the UM05-2X/6-311+g(2d,2p) level of theory. Energies relative to the dissociated phenoxy radical **1** and water (kcal/mol) and selected bond distances (Å).

transition state (TS), the O–H bond in water is elongated from 0.97 to 1.41 Å. The formation of the complex between OH and phenol from complex **A** is calculated to be endothermic by 31.5 kcal/mol, which is roughly the difference between the OH bond dissociation energies of water and phenol. For the reverse reaction, an activation barrier of 5.1 kcal/mol is estimated, which should kinetically stabilize the phenol–OH dimer in matrices at very low temperatures.

**Dynamic Simulations.** The stability of a  $\pi$ -complex between the phenoxy radical **1** and the water (dimer **C**) was investigated by dynamic simulations in both the gas phase and a simulated argon matrix. The starting point for the simulations was generated by removing a hydrogen atom from the  $\pi$ -complex between phenol **4** and water (dimer **F** in Figure 3). The quantum mechanics (QM) molecular dynamics (MD) simulations reveal that even at 7 K the initial  $\pi$ -complex is unstable in the gas phase and rearranges during the first ps to form the most stable dimer **A** (Figure 5). Similar simulations with different starting geometries with water interacting with the  $\pi$ -system of **1** lead to the same result. This clearly indicates that a  $\pi$ -complex **C** clearly does not exist as a minimum in the  $\text{I}\cdots\text{H}_2\text{O}$  system. This is in remarkable contrast to the  $4\cdots\text{H}_2\text{O}$  system, where the corresponding  $\pi$ -complex **F** is clearly a minimum (Figure 3).<sup>33</sup>

Although the  $\pi$ -complex is not stable in the gas phase, it might be stabilized in a matrix cage by the surrounding argon atoms. Therefore, the behavior of the  $\pi$ -complex was also investigated in a simulated argon matrix by classical MD simulations, quantum mechanics/molecular mechanics [(QM-(UB3LYP-D2/SVP)/CHARMM and QM(UB3LYP-D2/TZVPP)/CHARMM) optimizations, and quantum mechanics/molecular mechanics molecular dynamics [QM(UB3LYP-D2/SVP)/CHARMM] simulations.

Several setups were used to study the dynamics of matrix-isolated complexes between **1** and water: (i) Complex **A** was placed in the argon box, at a constant temperature of 7 K, and the simulation was run for 10 ps (Figures 6 and 7a). (ii) Complex **C** (Figure 5, first frame) was placed in the argon box at a constant temperature of 7 K for 10 ps (Figure 7b). (iii) The final frame obtained with setup ii was sampled under the same conditions for an additional 4 ps to ensure equilibration. After that, the temperature was allowed to increase first from 7 to 20 K (0.2 ps) and then from 20 to 30 K (0.2 ps) to simulate an

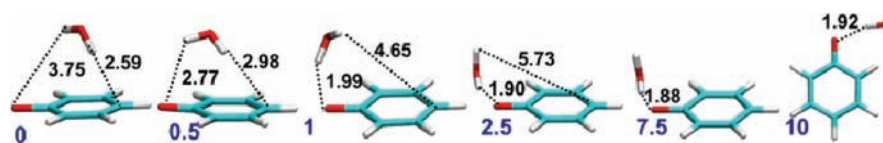


**Figure 5.** Snapshots taken from the QM MD simulation of the phenoxyl radical–water system in the gas phase at 7 K. The  $\text{OH1}_{\text{water}}\cdots\text{O}_{\text{radical}}$  and  $\text{OH2}_{\text{water}}\cdots\text{C}_{(\text{para})\text{radical}}$  distances (Å, in black) and the time (ps, in blue) are shown in the frames.

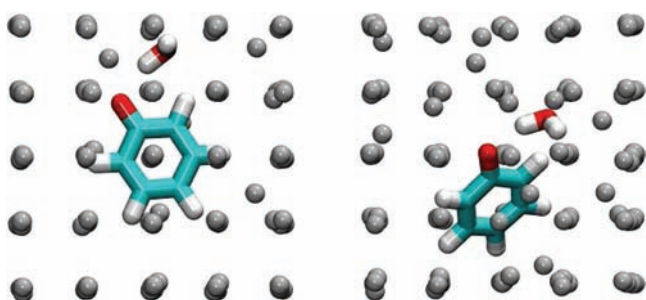


**Figure 6.** Embedding of complex A in argon. Frames taken after 10 ps at 7 K (left) and 30 K (right), respectively. The positions of the argon atoms are represented by the gray dots.

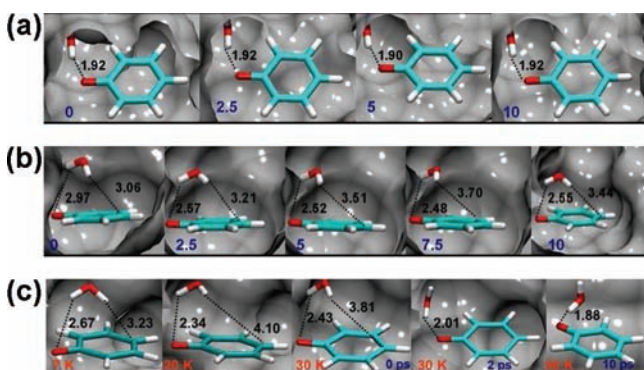


**Figure 7.** Snapshots from QM/MM MD simulations of complexes between **1** and water in argon. (a) Complex A in argon, 7 K, 10 ps. (b) Complex C in argon, 7 K, 10 ps. (c) Complex C in argon, temperature increasing in two stages from 7 to 20 K and from 20 to 30 K. Additional 10 ps were sampled at 30 K. The  $\text{OH1}_{\text{water}}\cdots\text{O}_{\text{radical}}$  distance (Å, in black) and the time (ps, in blue) are shown in the frames.

annealing process in the matrix. Finally, an additional 10 ps was sampled at 30 K (Figure 7c).

The simulations of phenoxyl radical **1** and water in argon reproduce the properties of argon matrices quite accurately. While at 7 K the argon atoms surrounding the trapped molecules are still highly ordered, a much larger disorder is found at 30 K (Figure 6). At this higher temperature, dimer A is able to rotate, whereas at 7 K, it is fixed with respect to the argon lattice. This is in accordance with observations of similar-sized molecules trapped in argon, which lose their orientation (measured by infrared dichroism)<sup>26,47,48</sup> rapidly at 30 K, whereas below 10 K, the orientation is persistent.

According to these simulations, dimer A is stable in an argon matrix at 7 K (Figure 7a) and at 30 K. In contrast, a water molecule positioned on top of **1** is bound by a very weak  $\text{OH}\cdots\pi$  interaction only (dimer C) and rearranges within 2 ps at 30 K to dimer A (Figure 7c). Only at very low temperature (7 K), dimer C is metastable and survives the first 10 ps. Because annealing is required to produce the complex between **1** and water in the matrix experiments, we conclude that complex C cannot be formed under these conditions.

**Assignment of the IR Spectra.** To characterize the complex between **1** and water that is formed under the conditions of matrix isolation, we compared the experimental IR spectrum with IR spectra from DFT calculations in the gas phase and with IR spectra calculated for a simulated argon matrix (Table 1, and Supporting Information). As described before, the formation of the complex between **1** and water results in a very large red shift of the OH stretching vibration of water ( $-169\text{ cm}^{-1}$ ) and in a moderate blue shift of the CO stretching vibration of **1** ( $+14.6\text{ cm}^{-1}$ ). As expected, for the van der Waals complex B, where the water hydrogen atoms are not involved in a hydrogen bond, at all levels of theory, only a very small red shift of the water OH stretching vibration is predicted [e.g.,  $-9.9\text{ cm}^{-1}$  at the UM052X/6-311++G(2d,2p) level of theory]. The calculated blue shift for the CO stretching vibration is also much smaller than in the experiment observed. This clearly rules out dimer B as the complex observed in the experiment.

Complex C can also be excluded, since it is only metastable in argon and nonexistent in the gas phase. Nevertheless, we optimized the metastable structures obtained in argon at 7 K at the QM(UB3LYP-D2/TZVPP)/CHARMM level of theory to calculate a vibrational spectrum that can be compared to the experiment. The optimization leads to a very weak van der Waals complex, where the water molecule is displaced even further away from the oxygen atom of **1**. This structure is stabilized by the surrounding argon atoms and shows no direct interactions between the water and the  $\pi$ -system of **1** (dimer C, Figure 8). Consequently, the vibrational modes are very close

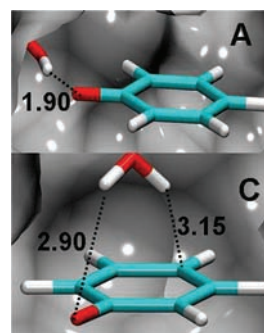


**Figure 8.** QM(UB3LYP-D2/TZVPP)/CHARMM optimized structures of dimers A and C.

to those of the isolated species, 3799.6 and 1486.5  $\text{cm}^{-1}$  for the OH and CO stretching vibrations, respectively, which allows discarding dimer C as responsible for the experimentally observed spectral shifts (see also Supporting Information).

Thus, complex A is the only remaining structure, and indeed, both the DFT and the QM/MM calculated vibrational frequencies match the observed bands of the  $\text{1}\cdots\text{H}_2\text{O}$  complex (Table 1). In particular, the QM/MM frequencies in an argon box are in excellent agreement with the experimental data. The OH stretching mode of the water molecule in the complex

shows a frequency of  $3608\text{ cm}^{-1}$ , as compared to  $3800\text{ cm}^{-1}$  in the isolated water molecule, indicating a  $192\text{ cm}^{-1}$  red shift for the complex. The frequency for the CO stretching vibration in the complex is  $1502\text{ cm}^{-1}$ , as compared to  $1480\text{ cm}^{-1}$  in the isolated phenoxyl radical **1**. This corresponds to a blue shift of  $22\text{ cm}^{-1}$ , in reasonable agreement with the experimental finding.

A similar blue shift of a carbonyl stretching vibration upon formation of a hydrogen bond with water was calculated for the complexes of the anion and dianion of *p*-benzoquinone **6** with two water molecules.<sup>49</sup> In these complexes, the blue shift was explained by a mixing of the carbonyl vibration with the bending vibration of water. This mixing is also observed in dimer **A**, where the CO stretching vibration also shows a small contribution of the water bending deformation (Figure 9). In neutral *p*-benzoquinone **6**, on the other hand, the formation of a hydrogen bond results in the expected red shift.<sup>49</sup>

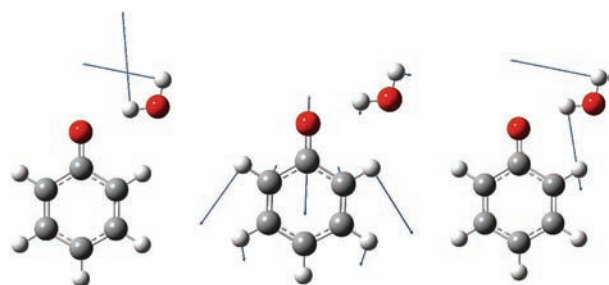


**Figure 9.** Displacement vectors illustrating three vibrations of the **1**...H<sub>2</sub>O dimer **A**. Left, water deformation vibration; center, CO stretching vibration coupled to the water deformation; and right, water rocking vibration.

## CONCLUSION

Both the experiments and the computations agree that an OH... $\pi$  complex between the water and the phenoxyl radical **1** (dimer **C**) does not exist as a minimum on the potential energy surface. Even if a  $\pi$ -interaction is enforced by enclosure in a rigid matrix cage (Figure 8), the nonbonding distances between the components are large, resulting in a weakly bound van der Waals complex, rather than a hydrogen-bonded dimer. Because the OH... $\pi$  complex **C** is no minimum, the binding energy of this configuration cannot be determined. However, the dynamic studies with a water molecule forced on top of the  $\pi$ -system of **1** reveal that there is only little interaction, resulting in extremely fast rearrangement, with no activation barrier, to dimer **A**.

It is instructive to compare the complexes in the **1**...H<sub>2</sub>O system with that in the **4**...H<sub>2</sub>O system. For the latter, a combined matrix isolation and theoretical study was recently published.<sup>33</sup> Three **4**...H<sub>2</sub>O complexes were described in this study: the most stable complex was, as expected, complex **D** with the acidic phenol as hydrogen bond donor and water as acceptor (Figure 3). This complex is stabilized by  $-5.68\text{ kcal/mol}$  at the B3LYP/6-311++G(2d,2p) level of theory, if BSSE corrections are included.<sup>33</sup> Dimer **D** is the only complex that was found in these matrix experiments<sup>33</sup> and is also the only one that is formed as a byproduct in our experiments. The second most stable dimer **E**, with water as hydrogen bond donor and the phenol oxygen atom as acceptor, corresponds to dimer **A** in the **1**...H<sub>2</sub>O system. The third dimer **F** is the rather

weak OH... $\pi$  complex, stabilized by only  $-1.69\text{ kcal/mol}$  [B3LYP/6-311++G(2d,2p) including BSSE].<sup>33</sup>

To directly compare the complexes of radical **1** with that of phenol **4** with water, we calculated the stabilization energies of all complexes at the same (U)M05-2X/6-311++G(2d,2p) level of theory (Figure 3). Dispersion corrections are implicitly considered in the M05-2X functional; it is therefore suitable for calculating weak interactions in open shell systems.<sup>50</sup> The **4**...H<sub>2</sub>O dimers **D**, **E**, and in particular **F** are slightly more stable with the M05-2X functional than with B3LYP (without empirical dispersive energy correction), indicating that dispersion interactions might contribute to the stabilization of these complexes.

The interesting finding of this comparison is that the most stable **1**...H<sub>2</sub>O dimer **A** ( $-7.41\text{ kcal/mol}$  including BSSE) is even slightly more stable than the most stable **4**...H<sub>2</sub>O dimer **D** ( $-6.72\text{ kcal/mol}$ ), where water is the hydrogen bond acceptor. This reflects the stronger basicity and weaker acidity of **1** as compared to **4**. With a dissociation energy of only  $4.45\text{ kcal/mol}$ , the **4**...H<sub>2</sub>O dimer **E** is  $3\text{ kcal/mol}$  less stable than the corresponding **1**...H<sub>2</sub>O complex **A**. This finding can be rationalized by comparing the calculated natural atomic charges for **1** with that of **4** (Table S3 in the Supporting Information). In **4**, the negative charge at the phenol oxygen atom is largely compensated by the positive charge of the phenolic hydrogen atom, making this oxygen atom less basic than the phenoxyl oxygen atom. This is also nicely illustrated by the electrostatic potential maps of **1** and **4** (Figure 10). The higher negative

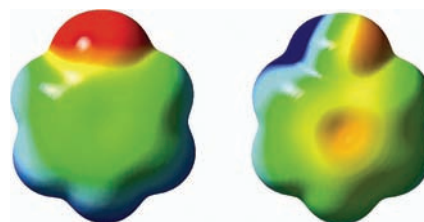


**Figure 10.** Electrostatic potential (red,  $-4 \times 10^{-2}$  a.u.; blue,  $+4 \times 10^{-2}$  a.u.) mapped on a surface of constant electron density ( $0.02\text{ electrons}/\text{\AA}^3$ ) for the phenoxyl radical **1** (left) and phenol **4** (right).

electrostatic potential at the phenoxyl oxygen atom as compared to the phenol oxygen atom clearly indicates that **1** is a much better hydrogen bond acceptor than **4**. The electrostatic maps also indicate that the  $\pi$ -system of **4** is a better acceptor than that of **1**, but the oxygen atom of **4** is still a better acceptor than its  $\pi$ -system. On the other hand, **4** is a much better hydrogen bond donor than **1**. Thus, the relative order of stabilities of water complexes expected from the qualitative interpretation of the electrostatic maps nicely agrees with the thermochemical estimations from the DFT calculations.

These findings are important to understand the basic changes in the intermolecular interactions when tyrosine is oxidized to the tyrosyl radical in biological systems. The CO stretching vibration of the tyrosyl radical in PSII was observed at  $1477\text{ cm}^{-1}$  using difference FTIR spectroscopy.<sup>20</sup> This value is quite close to the  $1480\text{ cm}^{-1}$  for matrix-isolated **1**, which suggests that **1** indeed is a useful model for the tyrosyl radical. By carefully studying the interactions within the protein surrounding including isotopic labeling, it should be possible to differentiate between a "free" and a hydrogen-bonded tyrosyl radical; the latter we predict to be blue-shifted in the order of

$15\text{ cm}^{-1}$ . This shift should be large enough for investigating the resolution of the tyrosyl radical after oxidation of tyrosine by time-resolved spectroscopy. While the phenolic part of tyrosine is a strong hydrogen bond donor and a weak hydrogen bond acceptor, this is reversed after oxidation, and a strong hydrogen bond acceptor is formed. Hydrogen bonds to the  $\pi$ -system of tyrosine might play a minor role for their stabilization, but after oxidation, no stabilization via  $\pi$ -interactions will remain. Hydrogen bonds to the  $\pi$ -system of tyrosyl radicals are not expected to be of any importance in biological systems.

## MATERIALS AND METHODS

**Materials.** Allyl phenyl ether **2** was purchased from ABCR (97% purity) and directly used for the matrix experiments without further purification.  $d_6$ -Phenol ( $d_6$ -4) was purchased from Aldrich (99% atom D) and used for the synthesis of  $d_5$ -allyl phenyl ether ( $d_5$ -2).

**Synthesis of  $d_5$ -2.**  $d_5$ -Allyl phenyl ether ( $d_5$ -2) was synthesized following a literature procedure.<sup>51</sup> Data for  $d_5$ -2: colorless oil.  $^1\text{H}$  NMR (200 MHz,  $\text{CDCl}_3$ ):  $\delta$  4.42 (m, 2H), 5.14–5.34 (m, 1H), 5.86–6.05 (m, 2H).  $^{13}\text{C}$  NMR (50.1 MHz,  $\text{CDCl}_3$ ):  $\delta$  68.7, 114.4 (t), 117.5, 120.3 (t), 128.9 (t), 133.4, 158.6.

**Matrix Isolation.** Matrix isolation experiments were performed by standard techniques using an APD HC-4 closed cycle helium compressor for cooling to 10 K or a Sumitomo compressor and coldhead for cooling to 3 K. FVP was carried out by slow deposition of **2** through a 9 cm quartz tube heated electrically with a tantalum wire. Compound **2** was degassed several times before doing FVP. The complexes between **1** and water were generated by codeposition of **1** and 0.1–1% water with a large excess of argon (Messer Griesheim, 99.99%) on top of a cold CsI window with a flow rate of approximately 1.70 sccm.

After deposition at 3 or 10 K, the matrices were annealed at temperatures above 25 K either by keeping the matrix at a fixed temperature for several minutes or by warming with an approximate rate of 1 K/min. After this annealing procedure, the matrices were cooled back to 3 or 10 K, respectively. Infrared spectra in the range between 400 and 4000  $\text{cm}^{-1}$  were recorded on FTIR spectrometers with 0.5  $\text{cm}^{-1}$  resolution. In the range 200–400  $\text{cm}^{-1}$ , a vacuum FTIR spectrometer equipped with an FIR beam splitter and CsI windows was used.

**DFT Calculations.** B3LYP<sup>41–45</sup> and M05-2X<sup>46</sup> density functionals were used as implemented in Gaussian 09 Revision B.01<sup>52</sup> and the B3LYP functional with empirical dispersive energy correction (UB3LYP-D2)<sup>44,45</sup> using Turbomole (version 5.10).<sup>53</sup> Pople's 6-311++G(2d,2p) basis set<sup>54</sup> was used for the geometry optimizations and calculations of the vibrational spectra. The stabilization energies were calculated by subtracting the energies of the monomers from those of the complexes and including ZPE corrections. The energies were also corrected for the basis set superposition errors (BSSE) using the counterpoise (CP) scheme of Boys and Bernardi.<sup>45</sup> For the IRC calculations, the phenoxyl radical and water monomers were used as reference, with the TS structure as a starting point.

**Dynamic Simulations.** QM MD simulations were performed using the program ChemShell<sup>55,56</sup> as an interface to Turbomole (version 5.10)<sup>53</sup> for the QM MD calculations, for which the B3LYP density functional<sup>41–43</sup> with empirical dispersive energy correction (B3LYP-D2)<sup>44</sup> and the SVP basis set<sup>57</sup> was used. The UB3LYP-D2/MD simulations were performed during 10 ps with a time step of 1 fs under NVT (canonical) conditions with a temperature of 7 K. A Nose–Hoover chain (NHC) thermostat<sup>58</sup> was used.

For the simulations of the phenoxyl radical–water complexes in an argon matrix, an argon box consisting of 4000 argon atoms was created manually using the lattice parameter  $a_0$  equal to 5.256 Å, which corresponds to the face-centered cubic crystal structure and the experimental density of 1.83  $\text{g}/\text{cm}^3$  obtained at 4.2 K for solid argon.<sup>59</sup> The CHARMM force field<sup>60</sup> formula for the Lennard–Jones (LJ) potential was used for Ar–Ar and Ar–X (X: nonargon atom) interactions with  $^{\text{Ar}}r_{\text{min}}$  equal to 3.83 Å and  $\epsilon$  equal to 0.241843 kcal/

mol (values associated with the parameter set HFDI by Ahlrichs et al.).<sup>61</sup> We used those parameters since they better reproduced the experimental density of solid argon during the NPT calculations (see the following).

As a first approach, MD simulations were performed using the NAMD program<sup>62</sup> and periodic boundary conditions. The argon box without the complex was first subjected to equilibration at a constant temperature of 7 K and constant zero pressure for 5 ns. The Berendsen barostat and simple temperature rescaling were used to ensure the NPT ensemble. During the 5 ns, the volume of the Ar box adjusted to its equilibrium value, giving nearly the experimental density for the solid argon.

In setups i and ii, the phenoxyl radical–water complex was manually inserted into the center of the equilibrated box (Figure 6), and all of the argon atoms lying too close to the phenoxyl radical and water atoms (within the half of the sum of  $r_{\text{min}}$  values of the nearby elements) were removed. The resulting system was further subjected to a 5 ns NPT simulation with the phenoxyl radical–water complex frozen. The standard CHARMM<sup>60</sup> LJ parameters for the TIP3P water model and phenylalanine side chain atom types were used for the phenoxyl radical and a water molecule.

The final structures from these MD simulations were subjected to a QM/MM optimization using the ChemShell program and the HDLCopt optimizer.<sup>63</sup> All of the atoms of the phenoxyl radical and the water molecule were treated at a QM level (B3LYP/SVP), and all argon atoms within 10 Å from the QM atoms were allowed to freely move during the optimization. The rest of the system was kept frozen. The optimized structures were then subjected to QM/MM MD simulations at the QM(UB3LYP-D2/SVP)/CHARMM level with constant temperature of 7 K, controlled by the Nose–Hoover thermostat for 10 ps (with a 1 fs step size).

The final structures from the first 10 ps MD of the both complexes (A and C, so that both maintained their initial orientation) were subjected to QM/MM optimizations at a QM(UB3LYP-D2/TZVPP)/CHARMM theory level. Numerical analyses of the vibration normal modes as implemented in ChemShell were performed for the resulting minima structures. Although no MD simulations were performed for the phenoxyl radical and water monomers in the argon box, both monomers were separately inserted into the previously equilibrated argon boxes and optimized at the same QM/MM level of theory that the complexes. The vibration normal-mode analysis was also performed for the monomers.

## ASSOCIATED CONTENT

### Supporting Information

IR spectra of the products of the FVP of allyl phenyl ether and  $d_5$ -allyl phenyl ether, IR spectra of  $d_5$ -phenoxyl radical interacting with  $\text{H}_2\text{O}$  and  $\text{D}_2\text{O}$ , tables with vibrational data of monomers and isotopomers, and table showing the natural atomic charges of phenol and the phenoxyl radical. This material is available free of charge via the Internet at <http://pubs.acs.org>.

## AUTHOR INFORMATION

### Corresponding Author

wolfram.sander@rub.de; esanchez@kofo.mpg.de

### Notes

The authors declare no competing financial interest.

## ACKNOWLEDGMENTS

This work was financially supported by the Deutsche Forschungsgemeinschaft (Forschergruppe 618) and the Fonds der Chemischen Industrie. E.S.-G. thanks Prof. Walter Thiel for his support and the computational resources, and the Fonds der Chemischen Industrie for a Liebig Stipend.

## REFERENCES

- (1) Jeffrey, G. A. *An Introduction to Hydrogen Bonding*; Oxford University Press: New York, 1997.
- (2) Desiraju, G. R. *Acc. Chem. Res.* **2002**, *35*, 565–573.
- (3) Crespo-Otero, R.; Sanchez-Garcia, E.; Suardiaz, R.; Montero, L. A.; Sander, W. *Chem. Phys.* **2008**, *353*, 193–201.
- (4) Yamaji, T.; Saiful, I. S. M.; Baba, M.; Yamauchi, S.; Yamauchi, J. *Bull. Chem. Soc. Jpn.* **2009**, *82*, 58–64.
- (5) Mardyukov, A.; Sanchez-Garcia, E.; Crespo-Otero, R.; Sander, W. *Angew. Chem., Int. Ed.* **2009**, *48*, 4804–4807.
- (6) An, X.; Liu, H.; Li, Q.; Gong, B.; Cheng, J. J. *Phys. Chem. A* **2008**, *112*, 5258–5263.
- (7) Hernandez-Soto, H.; Weinhold, F.; Francisco, J. S. *J. Chem. Phys.* **2007**, *127*, 164102/1–164102/10.
- (8) Torrent-Sucarrat, M.; Anglada, J. M. *ChemPhysChem* **2004**, *5*, 183–191.
- (9) Wang, B.-Q.; Li, Z.-R.; Wu, D.; Hao, X.-Y.; Li, R.-J.; Sun, C.-C. *Chem. Phys. Lett.* **2003**, *375*, 91–95.
- (10) Lucarini, M.; Mugnaini, V.; Pedulli, G. F.; Guerra, M. J. *Am. Chem. Soc.* **2003**, *125*, 8318–8329.
- (11) Mardyukov, A.; Crespo-Otero, R.; Sanchez-Garcia, E.; Sander, W. *Chem.—Eur. J.* **2010**, *16*, 8679–8689.
- (12) Lai, C.-H.; Chou, P.-T. *J. Comput. Chem.* **2007**, *28*, 1357–1363.
- (13) Solimannejad, M.; Alikhani, M. E. *Chem. Phys. Lett.* **2005**, *406*, 351–354.
- (14) Engdahl, A.; Nelander, B. *J. Chem. Phys.* **2005**, *122*, 126101/1–126101/2.
- (15) Engdahl, A.; Nelander, B. *Phys. Chem. Chem. Phys.* **2004**, *6*, 730–734.
- (16) Wanke, R.; Benisvy, L.; Kuznetsov, M. L.; da Silva, M. F.; Pombeiro, A. J. *Chemistry* **2011**, *17*, 11882–11892.
- (17) McDonald, W. J.; Einarsdottir, O. *J. Phys. Chem. B* **2010**, *114*, 6409–6425.
- (18) Engstroem, M.; Himo, F.; Graeslund, A.; Minaev, B.; Vahtras, O.; Agren, H. *J. Phys. Chem. A* **2000**, *104*, 5149–5153.
- (19) Bernard, M. T.; MacDonald, G. M.; Nguyen, A. P.; Debus, R. J.; Barry, B. A. *J. Biol. Chem.* **1995**, *270*, 1589–1594.
- (20) Kim, S.; Ayala, I. I.; Steenhuis, J. J.; Gonzalez, E. T.; Barry, B. A. *Biochim. Biophys. Acta* **1998**, *1364*, 337–360.
- (21) Sjöholm, J.; Havelius, K. G.; Mamedov, F.; Styring, S. *Biochemistry* **2009**, *48*, 9393–9404.
- (22) Stone, T. J.; Waters, W. A. *J. Chem. Soc.* **1964**, 213.
- (23) Tripathi, G. N. R.; Sun, Q.; Armstrong, D. A.; Chipman, D. M.; Schuler, R. H. *J. Phys. Chem. A* **1992**, *96*, 5344–5350.
- (24) Lloyd, R. V.; Wood, D. E. *J. Am. Chem. Soc.* **1974**, *96*, 659.
- (25) Dewar, M. J. S.; David, D. E. *J. Am. Chem. Soc.* **1980**, *102*, 7387.
- (26) Radziszewski, J. G.; Gil, M.; Gorski, A.; Spanget-Larsen, J.; Waluk, J.; Mróz, B. *J. Chem. Phys.* **2001**, *115*, 9733.
- (27) Shindo, H.; Hiraishi, J. *Chem. Phys. Lett.* **1981**, *80*, 238.
- (28) Giuliano, B. M.; Reva, I.; Lapinski, L.; Fausto, R. *J. Chem. Phys.* **2012**, *136*, 024505/1–024505/2.
- (29) Spanget-Larsen, J.; Gil, M.; Gorski, A.; Blake, D. M.; Waluk, J.; Radziszewski, J. G. *J. Am. Chem. Soc.* **2001**, *123*, 11253.
- (30) Friderichsen, A. V.; Shin, E. J.; Evans, R. J.; Nimlos, M. R.; Dayton, D. C.; Ellison, G. B. *Fuel* **2001**, *80*, 1747–1755.
- (31) Fisher, I. P.; Palmer, T. F.; Lossing, F. P. *J. Am. Chem. Soc.* **1964**, *86*, 2741–2742.
- (32) Nandi, S.; Arnold, P. A.; Carpenter, B. K.; Nimlos, M. R.; Dayton, D. C.; Ellison, G. B. *J. Phys. Chem. A* **2001**, *105*, 7514–7524.
- (33) Gor, G. Y.; Tapio, S.; Domanskaya, A. V.; Rasanen, M.; Nemukhin, A. V.; Khriachtchev, L. *Chem. Phys. Lett.* **2011**, *517*, 9–15.
- (34) Sander, W.; Bucher, G.; Wierlacher, S. *Chem. Rev.* **1993**, *93*, 1583–1621.
- (35) Ayers, G. P.; Pullin, A. D. E. *Spectrochim. Acta, Part A* **1976**, *32A*, 1629–1639.
- (36) Ayers, G. P.; Pullin, A. D. E. *Spectrochim. Acta, Part A* **1976**, *32A*, 1641–1650.
- (37) Mann, B.; Neikes, T.; Schmidt, E.; Luck, W. A. P. *Ber. Bunsen-Gesellschaft* **1974**, *78*, 1236–1241.
- (38) Ayers, G. P.; Pullin, A. D. E. *Spectrochim. Acta, Part A* **1976**, *32A*, 1695–1704.
- (39) A complex between the ally radical and the water was observed in this study. Details will be published elsewhere.
- (40) Sander, W. W. *J. Org. Chem.* **1988**, *53*, 2091–2093.
- (41) Dirac, P. A. M. *Proc. R. Soc. London, Ser. A* **1929**, *123*, 714–733.
- (42) Slater, J. C. *Phys. Rev.* **1951**, *81*, 385–390.
- (43) Becke, A. D. *Phys. Rev. A* **1988**, *38*, 3098–3100.
- (44) Grimme, S. *J. Comput. Chem.* **2004**, *25*, 1463–1473.
- (45) Grimme, S. *J. Comput. Chem.* **2006**, *27*, 1787–1799.
- (46) Zhao, Y.; Schultz, N. E.; Truhlar, D. G. *J. Chem. Theory Comput.* **2006**, *2*, 364–382.
- (47) Neuhaus, P.; Grote, D.; Sander, W. *J. Am. Chem. Soc.* **2008**, *130*, 2993–3000.
- (48) Michl, J.; Thulstrup, E. W. *Acc. Chem. Res.* **1987**, *20*, 192–199.
- (49) Manojkumar, T. K.; Choi, H. S.; Tarakeswar, P.; Kim, K. S. *J. Chem. Phys.* **2003**, *118*, 8681.
- (50) Zhao, Y.; Truhlar, D. G. *Acc. Chem. Res.* **2008**, *41*, 157–167.
- (51) Murakami, H.; Minami, T.; Ozawa, F. *J. Org. Chem.* **2004**, *69*, 4482–4486.
- (52) Frisch, M. J.; Trucks, G. W.; Schlegel, H. B.; Scuseria, G. E.; Robb, M. A.; Cheeseman, J. R.; Scalmani, G.; Barone, V.; Mennucci, B.; Petersson, G. A.; Nakatsuji, H.; Caricato, M.; Li, X.; Hratchian, H. P.; Izmaylov, A. F.; Bloino, J.; Zheng, G.; Sonnenberg, J. L.; Hada, M.; Ehara, M.; Toyota, K.; Fukuda, R.; Hasegawa, J.; Ishida, M.; Nakajima, T.; Honda, Y.; Kitao, O.; Nakai, H.; Vreven, T.; Montgomery, J. A., Jr.; Peralta, J. E.; Ogliaro, F.; Bearpark, M.; Heyd, J. J.; Brothers, E.; Kudin, K. N.; Staroverov, V. N.; Kobayashi, R.; Normand, J.; Raghavachari, K.; Rendell, A.; Burant, J. C.; Iyengar, S. S.; Tomasi, J.; Cossi, M.; Rega, N.; Millam, J. M.; Klene, M.; Knox, J. E.; Cross, J. B.; Bakken, V.; Adamo, C.; Jaramillo, J.; Gomperts, R.; Stratmann, R. E.; Yazyev, O.; Austin, A. J.; Cammi, R.; Pomelli, C.; Ochterski, J. W.; Martin, R. L.; Morokuma, K.; Zakrzewski, V. G.; Voth, G. A.; Salvador, P.; Dannenberg, J. J.; Dapprich, S.; Daniels, A. D.; Farkas, O.; Foresman, J. B.; Ortiz, J. V.; Cioslowski, J.; Fox, D. J. *Gaussian 09*, revision B.01; Gaussian, Inc.: Wallingford, CT, 2009.
- (53) Ahlrichs, R.; Baer, M.; Haeser, M.; Horn, H.; Koelmel, C. *Chem. Phys. Lett.* **1989**, *93*, 165–169.
- (54) Krishnan, R.; Binkley, J. S.; Seeger, R.; Pople, J. A. *J. Chem. Phys.* **1980**, *72*, 650–654.
- (55) ChemShell, a Computational Chemistry Shell; see [www.chemshell.org](http://www.chemshell.org).
- (56) Sherwood, P.; de, V. A. H.; Guest, M. F.; Schreckenbach, G.; Catlow, C. R. A.; French, S. A.; Sokol, A. A.; Bromley, S. T.; Thiel, W.; Turner, A. J.; Billeter, S.; Terstegen, F.; Thiel, S.; Kendrick, J.; Rogers, S. C.; Casci, J.; Watson, M.; King, F.; Karlsen, E.; Sjøvoll, M.; Fahmi, A.; Schafer, A.; Lennartz, C. *J. Mol. Struct.: THEOCHEM* **2003**, *632*, 1–28.
- (57) Weigend, F.; Haser, M.; Patzelt, H.; Ahlrichs, R. *Chem. Phys. Lett.* **1998**, *294*, 143–152.
- (58) Senn, H. M.; Thiel, S.; Thiel, W. *J. Chem. Theory Comput.* **2005**, *1*, 494–505.
- (59) Henshaw, D. G. *Phys. Rev.* **1958**, *111*, 1470–1475.
- (60) MacKerell, A. D., Jr.; Bashford, D.; Bellott, M.; Dunbrack, R. L.; Evanseck, J. D.; Field, M. J.; Fischer, S.; Gao, J.; Guo, H.; Ha, S.; Joseph-McCarthy, D.; Kuchnir, L.; Kuczera, K.; Lau, F. T. K.; Mattos, C.; Michnick, S.; Ngo, T.; Nguyen, D. T.; Prodhom, B.; Reiher, W. E., III; Roux, B.; Schlenkerich, M.; Smith, J. C.; Stote, R.; Straub, J.; Watanabe, M.; Wiorkiewicz-Kuczera, J.; Yin, D.; Karplus, M. *J. Phys. Chem. B* **1998**, *102*, 3586–3616.
- (61) Ahlrichs, R.; Penco, R.; Scoles, G. *Chem. Phys.* **1977**, *19*, 119–130.
- (62) Phillips, J. C.; Braun, R.; Wang, W.; Gumbart, J.; Tajkhorshid, E.; Villa, E.; Chipot, C.; Skeel, R. D.; Kale, L.; Schulten, K. *J. Comput. Chem.* **2005**, *26*, 1781–1802.
- (63) Billeter, S. R.; Turner, A. J.; Thiel, W. *Phys. Chem. Chem. Phys.* **2000**, *2*, 2177–2186.
- (64) Ayers, G. P.; Pullin, A. D. E. *Chem. Phys. Lett.* **1974**, *29*, 609–615.

(65) Engdahl, A.; Nelander, B. *J. Mol. Struct.* **1989**, *193*, 101–109.